

Strain Rate Effect on Strain Localization in Alloy 718 Ni-Based Superalloy at Intermediate Temperature

Malo Jullien, R. L. Black, J. C. Stinville, Marc Legros, and Damien Texier

Abstract

Tensile tests on Alloy 718 Ni-based superalloy at 650 °C at different strain rates revealed a strain-rate dependency on the fracture mode. A change from intergranular to transgranular fracture was observed in air as the strain rate increased, mainly when Portevin-Le-Chatelier (PLC) mesoscopic deformation bands were present. To better understand the link between strain rate and fracture mode, a description of the strain localization in the early deformation stage is needed. In this study, high-resolution digital image correlation (HR-DIC) was carried out at the onset of strain localization, a low strain rate (LSR, $\dot{\epsilon} = 10^{-4} \text{ s}^{-1}$) and at high strain rate (HSR, $\dot{\epsilon} = 10^{-2} \text{ s}^{-1}$). This latter condition aimed at investigating the microplasticity development within PLC bands. The in-plane and out-of-plane displacement components of each single plastic event were measured to accurately assess and distinguish morphological sliding at grain boundaries (i.e., grain boundary sliding) and dislocation slip. The deformation within the PLC bands was examined at macro, meso, and microscales. Statistical analyses highlighted the distribution and partitioning of these strain localization events related to different microstructural features, including grains, and grain and twin boundaries. Grain boundary sliding was found to be more prominent at LSR. Interestingly, events near and parallel to twin boundaries are particularly intense regardless of the strain rate. At HSR, grain boundary sliding is less pronounced, and a high density of intragranular slip bands

M. Jullien (⋈) · D. Texier

Institut Clement Ader—CNRS UMR 5312, 81013 Albi Cedex 09,

France

e-mail: malo.jullien@mines-albi.fr

M. Jullien \cdot M. Legros

Centre d'Elaboration de Matériaux et d'Etudes Structurales, CNRS UPR 8011, 31055 Toulouse Cedex 4, France

R. L. Black · J. C. Stinville

University of Illinois at Urbana-Champaign, Urbana, USA

developed within the PLC bands; based on observations before and after the occurrence of the PLC band.

Keywords

Digital image correlation • Ni-based superalloy • Slip localization • Grain boundary sliding • Portevin-Le-Chatelier

Introduction

Ni-based superalloy Alloy 718 (also reported InconelTM 718) is an excellent alloy candidate for structural components operating at intermediate temperatures (350– 650 °C). It owes its widespread use mainly to its chromiaforming layer and its excellent mechanical properties up to 650 °C [1, 2]. In the past decades, its mechanical behavior and damage behavior have been intensively investigated up to high temperatures to establish a relationship between its strain-rate sensitivity and its resistance to oxidation-assisted intergranular cracking (OAIC) [3–5]. At 650 °C and low strain rate, the environment greatly impacts the ductility and fracture behavior of the material. Indeed, transgranular fracture is reported for tensile tests performed under vacuum. In contrast, the fracture is fully or partially intergranular in air, accompanied by a significant drop in ductility [3]. In addition, tensile tests with Portevin-Le-Chatelier (PLC) instabilities show a lower ductility loss than tests performed at the same temperature but at a lower strain rate. The strain rate threshold at which PLC instabilities occur depends on the temperature regardless of the environmental condition [3]; at 650 °C, the strain-rate threshold ranges between 10^{-3} and 10^{-2} s⁻¹. When PLC occurs, i.e., at relatively high strain rates, the ductility is similar in air and under vacuum, and the fracture is transgranular in both cases. The current state of the art on PLC occurrence [6] agrees on the fact that the serration is caused by a negative strain-rate sensitivity (SRS), which itself is due to dynamic strain aging (DSA) in the case of superalloys. Dislocations are repeatedly blocked by Cottrell atmospheres and escape by stacking fault shearing. However, no model can predict the location of PLC bands during deformation.

At the grain level, it was observed at room temperature and 650 °C that Alloy 718 develops planar slip bands due to the repeated shearing of γ'' precipitates on primary octahedral slip planes [7]. In addition, previous work on Ni-based superalloys using high-resolution digital image correlation (HR-DIC) techniques to investigate creep properties at intermediate temperature [8–10], highlighted high strain localization at grain boundaries (GBs). Preliminary results evidenced that, under tensile loading, strain localization along GBs was insignificant from room temperature to 350 °C and dense at 650 °C [11]. Therefore, capturing strain partitioning at the microstructure level of Alloy 718 at 650 °C is critical to better understand the relationship between early strain localization, either transgranular or intergranular, and both PLC bands location and OAIC.

HR-DIC techniques using scanning electron microscopy (SEM) allow to accurately capture and identify slip localization at the sub-grain level for various materials at room temperature [12–14]. Studies on Ni-based super alloys [15–18] have established that $\Sigma 3$ annealing twin boundaries (TBs) are critical sites under cyclic loading at room temperature due to intense slip localization developing parallel to and near certain TBs. Under these test conditions, strain localization at TBs appears right from the early stages of deformation before intragranular slipping and intensifies with increasing macroscopic deformation. Several explanations were reported in the literature: (i) Material elastic anisotropy causes local stress concentrations near TBs, which significantly enhances dislocation slip [19, 20]; (ii) certain superalloys exhibit disruption in the precipitate state near TBs, contributing to increased slip localization and crack nucleation [21].

At intermediate temperature, several involved deformation processes are expected to induce competing strain localization at GBs, TBs, and intragranularly [9-11]; each localization event related to these microstructural features is more or less pronounced depending on the temperature and strain rate. The shearing associated with a slip event is along a crystallographic direction and can be measured solely using the in-plane kinematics field from HR-DIC measurements and local crystallographic information from EBSD measurements [12, 22]. For grain boundary sliding, the kinematics displacement at the GBs is morphological and depends on several microstructural parameters [23, 24]. Measurement of strain localization associated with grain boundary sliding requires both in-plane and out-of-plane information that conventional HR-DIC using SEM images cannot provide. Fortunately, complementary measurements of in-plane and out-ofplane measurements can be achieved using HR-DIC through ex-situ laser scanning confocal microscopy (LSCM) measurements [25].

The present study focuses on the effect of the strain rate on strain localization partitioning at GBs, TBs and intragranularly for Alloy 718 at 650 °C, in the PLC (high strain-rate (HSR)) and non-PLC (low strain-rate (LSR)) domains. Inplane HR-DIC analyses and out-of-plane measurements were concomitantly performed ex situ before and after PLC under tensile loading conditions at 650 °C. A statistical analysis was carried out to assess the evolution of strain localization related to microstructure with respect to PLC instabilities. A similar investigation at LSR was carried out to explore the effect of the strain rate on strain partitioning at the microstructural scale, with a special emphasis on the role of GBs in the deformation process. Assessment of strain partitioning at the microstructural scale is of critical importance for industrial application since it drives development of early damage under service.

Experimental Procedures

Material

The material tested in the present work is an Alloy 718 in the form of a rolled sheet with the following nominal composition: 18.57% Cr, 18% Fe, 5.02% Nb, 2.86% Mo, 0.11% Co, 0.58% Al, 0.97% Ti, and <0.01% Ta (weight percent). Flat dogbone-tensile specimens were first laser-machined from the rolled sheet, then heat treated at 1080 °C for 5 min (air quench), followed by two steps of aging at 720 °C then 620 °C, both for 8h. This heat treatment resulted in a fine $\gamma/\gamma'/\gamma''$ microstructure and a grain size distribution between 25 and 100 µm. The tensile specimens were mechanically polished down to colloidal silica for a mirror finish. The speckle pattern used for the HR-DIC was a thin chromium oxide obtained using a short-term pre-oxidation in air at 650 °C for 15 min. The resulting speckle pattern has a randomly distributed topography and gray levels, calquing the $\gamma/\gamma'/\gamma''$ microstructure. It is stable under a vacuum for hours at intermediate temperatures.

Interrupted Tensile Tests and HR-DIC

Tensile tests were performed at $650\,^{\circ}\text{C}$ under vacuum (10^{-5} mbar), the chamber being isolated using a sealed quartz tube with soft bellows. Heating was carried out using a resistive furnace with a center split design around the quartz tube. One set of specimens underwent tensile tests at a strain rate of $10^{-2}\,\text{s}^{-1}$ (HSR) and another at $10^{-4}\,\text{s}^{-1}$ (LSR). One monotonic test was first carried out at each strain rate to first obtain the macroscopic mechanical behavior. Then, interrupted tensile tests were performed and paired with ex-situ HR-DIC. For the LSR condition, one interruption was done at 0.2% of plas-

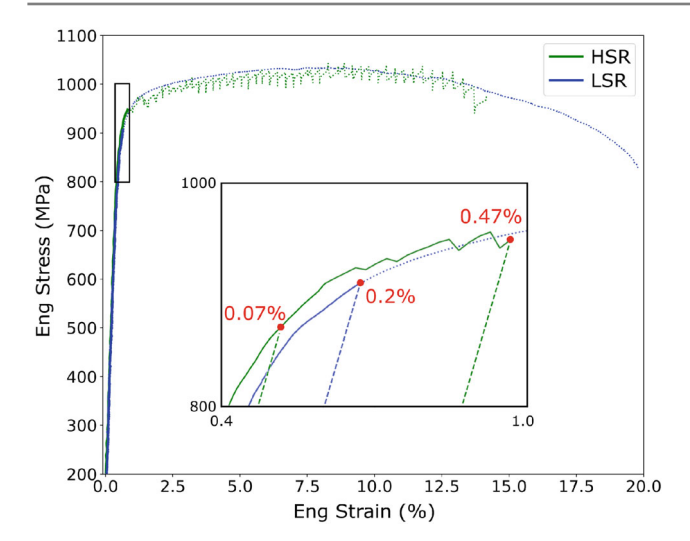


Fig. 1 Engineering stress-strain curves of the investigated material under vacuum. Solid lines are the interrupted tests and dashed lines are tests performed until rupture

tic strain. For the HSR condition, two interruptions were done, one at 0.07%, before the occurrence of PLC bands and the second at 0.47%, after the occurrence of three PLC bands. The corresponding stress-strain curves are illustrated in Fig. 1. The macroscopic strain was obtained using optical extensometry (macroscopic DIC). Optical images used for the HSR test are depicted in Fig. 2. HR-DIC was performed on high-resolution SEM images taken ex situ using a FEI Helios 600i field emission gun scanning electron microscope. For the specimen tested at LSR, an area of $1 \times 0.3 \text{ mm}^2$ was taken, while the region of interest was increased to $3 \times 0.3 \text{ mm}^2$ for the test performed at HSR. Maps are mosaics of SEM images which allowed to map large regions of interest with a spatial resolution compatible with the deformation mechanisms to capture. The DIC method used was Heaviside-DIC [12] (H-DIC). In addition to measuring the in-plane displacement field and derived strain fields, this technique also provides information on discontinuities within subsets of pixels. The information extracted is the amplitude of kinematics discontinuity and its angle relative to the macroscopic loading direction. This technique demonstrated its relevance for the identification of slip events from in-plane kinematics measurements [12]. Furthermore, height maps were collected using a laser scanning confocal microscope (LSCM) from Olympus (LEXT OLS5100). The laser scanning allows an in-plane spatial resolution lower than 120 nm and a resolution of 9 nm in the Z-direction. This technique enables accurate mapping of the sample topography and thus height discontinuities related to either slip events or GB sliding [26]. On both tensile specimens, confocal images covered almost the entire sample gauge area. In addition, EBSD data were collected using a JEOL JSM 7100F SEM and an Oxford EBSD SYMMETRY S2 system. Crystallographic orientations and grain boundaries information were extracted using the MTEX library [27].

Data Merging

The strategy used to merge the multimodal data acquired is (1) to align the data using a control point technique from the Argos package [28], (2) to identify the plastic events manually, and (3) to collect multimodal data using ImageJ tools. Events were automatically categorized as a function of microstructural features, i.e., intragranular slip, strain localization near and parallel to twin boundary, and grain boundary sliding. The number of events identified for each step is reported in Table 1. The statistical analysis was carried out on the merged dataset using a home-developed Python script. A portion of the dataset is presented in Fig. 3 showing in-plane strain localization using HR-DIC on SEM images and out-of-plane information using LSCM measurements in regard to the grain structure depicted with an EBSD map.

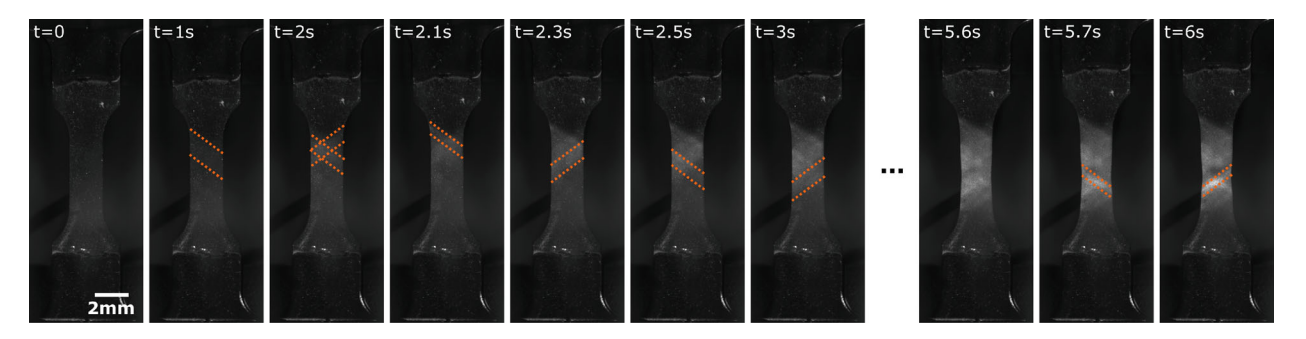


Fig. 2 Optical images of the sample gauge during a HSR tensile test performed at 650 °C under vacuum. Dotted orange lines highlight some PLC bands

Table 1 Summary of the strain state for every step.

	LSR	HSR	HSR	
	Step 1	Step 1	Step 2	
Strain rate (mm/s)	10^{-4}	10^{-2}	10^{-2}	
Strain level	0.2%	0.07%	0.47%	
Number of event analysed	1305	1155	3275	

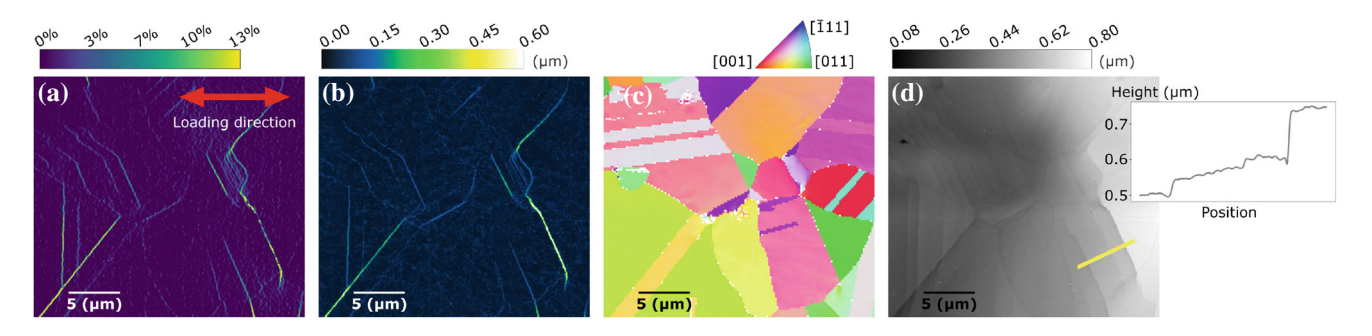


Fig. 3 Dataset presentation; a Strain map along the tensile direction. b In plane slip amplitude. c Inverse pole figure in the z-direction (IPFZ) of the corresponding area. d Height map with a profile plot along the yellow band

Results

High-Resolution DIC

Differences in tensile behavior were found between the two strain rates at 650 °C. The occurrence of a jerky flow specific to the PLC behavior appeared at HSR (Fig. 1). These serrations came with macroscopic inclined bands of intense strain, as shown on the optical images during the HSR tensile test (Fig. 2). The sample tested at LSR has a similar elastic behavior but does not experience serration and has a higher ductility. Interrupted tensile tests were carried out to capture the strain distribution within PLC bands before and after their occurrence. The corresponding tensile curves are displayed in the insert on Fig. 1. HR-DIC was performed on these interrupted tensile tests, and the resulting strain maps are shown in Fig. 4a and b for LSR and HSR, respectively. It is worth noting that only one-third of the strain field is shown for HSR for visualization purposes. It corresponds to the map after PLC bands (Fig. 4b). Strain maps show strain localization at GB and intragranular slip, regardless of the strain rate. Differences in strain localization amplitude and spatial distribution with respect to the microstructure can yet be evidenced at HSR and LSR and will be further investigated.

The strain map illustrated in Fig. 4b shows mesoscopic strain heterogeneities due to PLC bands; PLC bands experience more strain localization events. Two magnified regions, within and outside of the PLC bands, exhibit differences in the evolution of the strain state before and after the PLC occurrence. In PLC bands, several new events appeared between the two loading steps (Fig. 4c and d) when the stain localization

landscape remains nearly unchanged outside of the PLC bands (Fig. 4e and f). Inside PLC bands, the micro-plasticity developed is localized in the form of numerous but low-intensity intragranular slip bands. In contrast, outside of the PLC bands, few new plastic events are observed, and strain localization is amplified.

Strain Localization

Statistical analyses of strain localization events were performed to quantify microplasticity as a function of the microstructure. Each strain map's discrete plastic events (slip band or GB sliding) were identified and classified depending on their location, i.e., intragranular slip, slip near and parallel to a twin boundary, and grain boundary sliding. Plastic events were manually identified on strain maps, and each labeled event was projected on the EBSD map. Depending on their position, the corresponding events were classified as intragranular, TB, or GB. A TB classification means that the plastic event is a slip band closer than 2.5 µm from a twin boundary; a GB classification stands for a GB slipping; the intragranular class groups all slip bands inside the grains. The result of this statistical analysis is summarized on the bar chart in Fig. 5. On the y-axis, the amount of strain localization per area is plotted; the latter is considered as the slip/sliding amplitude multiplied by the length of the event. It is important to specify that the slip/sliding amplitude is measured in 3D; the displacement in the sample plane is measured by H-DIC and the out-of-plane displacement is measured by LSCM. For the LSR condition at a plastic strain level of 0.2, 43% of the strain

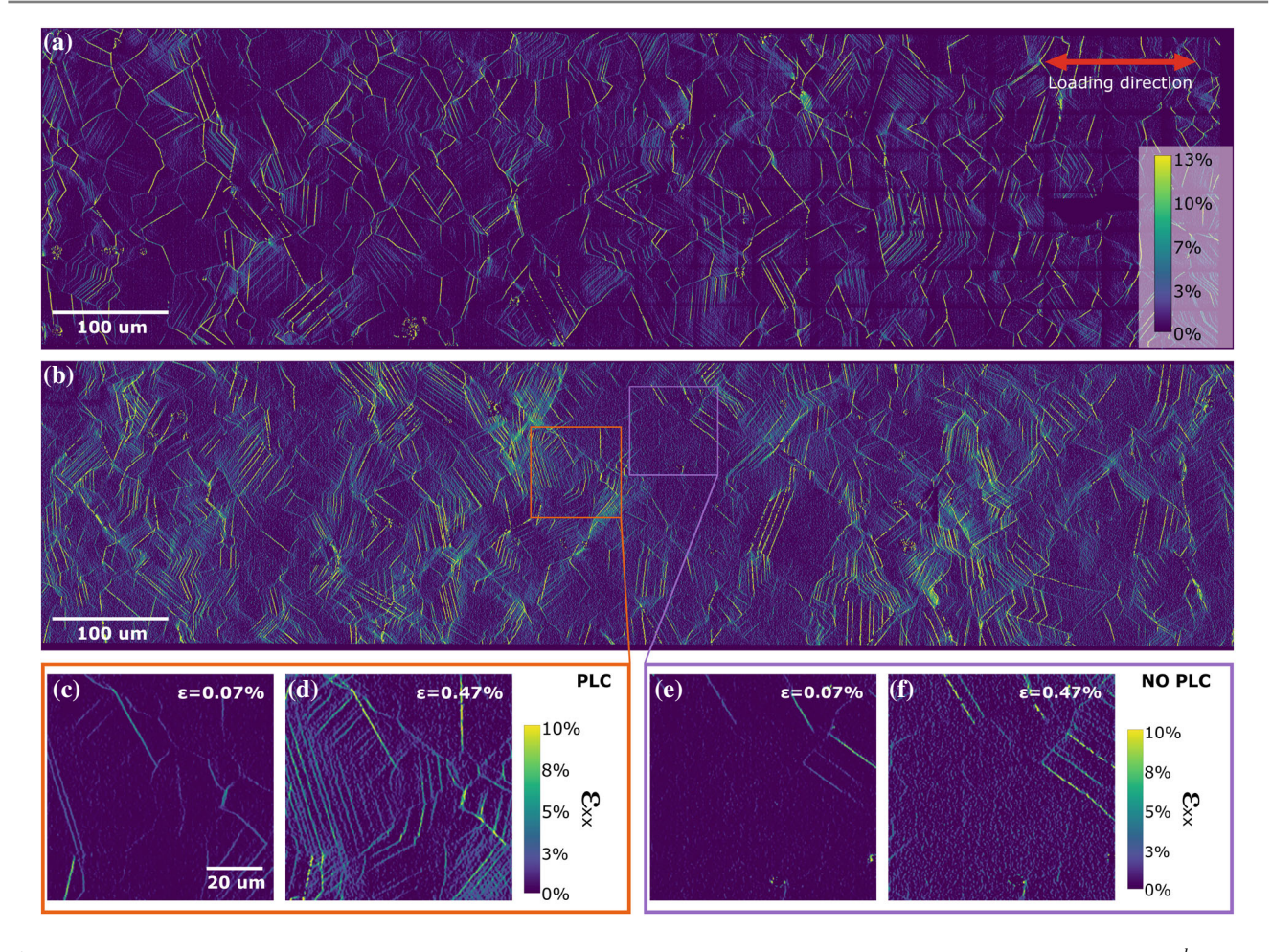


Fig. 4 Strain maps along the tensile direction obtained by H-DIC. **a** 0.2% of plastic strain at LSR. **b** 0.47% of plastic strain at HSR (2nd step, 1/3 of the map). **c** and **d** Magnified regions within a PLC band, before and after its occurrence, respectively; **e** and **f** Magnified region outside a PLC band, before and after its occurrence, respectively

localization is located at GBs. The remaining events are distributed between TBs (27%) and intragranular slip (30%). For the HSR condition, in the early stage of deformation (0.07% plastic strain), only 12% of the strain localization is located at GBs, and the rest is almost equally distributed between TBs and the interior of grains. When the strain increases, and PLC occurs, the strain partitioning changes. Strain localization at GBs decreased to 9.1% of the discrete microplasticity, and 56% corresponds to intragranular slip.

Tracking the evolution of the strain localization at HSR was possible by the two strain states captured by HR-DIC. The plastic strain added between the two steps can be separated into two categories: the increase in strain amplitude of existing plastic events (old events) and the strain localized as new plastic events. These two categories account for 35 and 65% of the amount of slip/sliding, respectively. Figure 6 shows the distribution of the amplitude increase between the two loading steps for each microstructural feature. As seen in Fig. 5 at the second step of the HSR test, 56% of the plastic events occurred as intragranular slip versus 35% for TBs

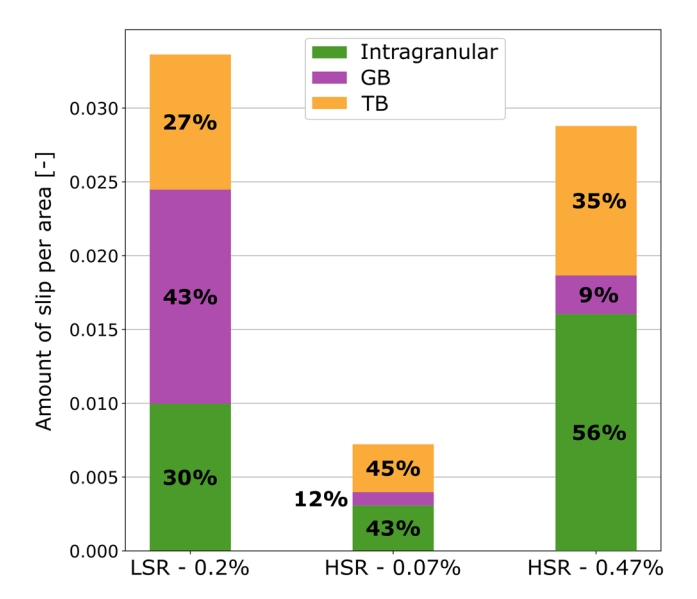


Fig. 5 Strain intensity partitioning for each tensile step at LSR and HSR. The percentage displayed on the x labels corresponds to the macroscopic strain at each step

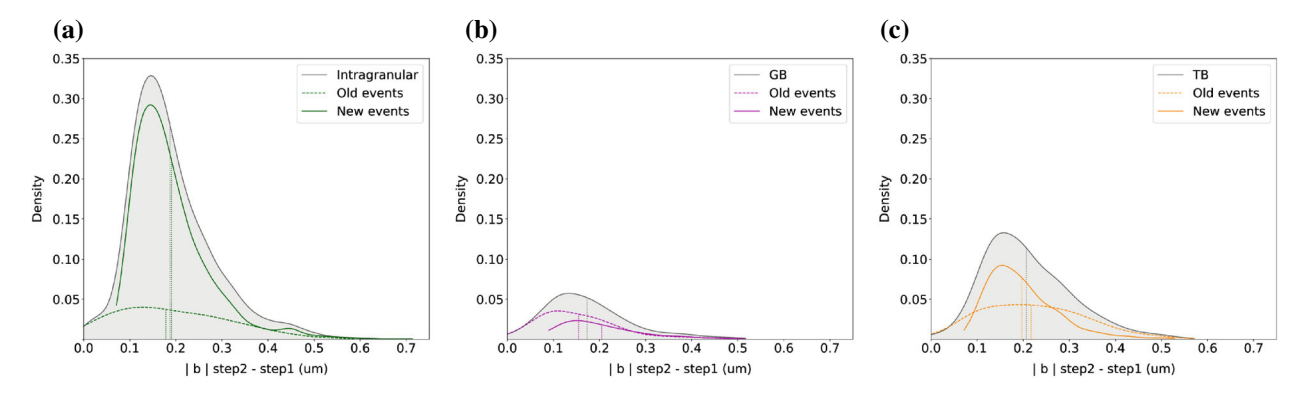


Fig. 6 Distribution of the slip amplitude increase for each microstructural feature at HSR; **a** inside the grains, **b** at grains boundaries, and **c** near twin boundaries. For each category, the gray areas are distributions of all the events, the solid lines are distributions of the events that were triggered between the two loading steps, and dashed lines are the distributions of events triggered in the early stage of deformation

and 9% for GBs. Thus, the density of the intragranular amplitude increase is much greater. A particular point to consider is the density difference between the old and new events. In Fig. 6a, the density of new events is much higher than that of old events. This indicates a much higher number of new events compared to old events. Most intragranular new events have low intensity, as shown by the maximum of the function located at 0.15 µm. Old intragranular events also have a low average slip amplitude increase of the same magnitude as the new events (0.18 µm). However, some intragranular events, old or new, were found to have a large amplitude increase. In contrast, the amplitude increase of the events at GBs is lower. Furthermore, fewer new events are triggered compared to the interior of grains or near TBs. Regarding the old events at GBs, they have a lower amplitude increase than everywhere else. Finally, the new events near TB are fewer than at the interior of grains but have about the same distribution. In contrast, the distribution of old events differs from the other locations. Indeed, a higher number of old events with a high slip amplitude increase can be found. It results in an average amplitude increase near TBs, which is slightly higher than in other locations.

A special interest was brought to the events with the highest slip amplitude increase between the two interruptions, before and after PLC occurrence. On the one hand, when considering the 10% of the events with the highest amplitude increase (Fig. 7), 26% are new intragranular slip events. This implies that, in addition to being numerous, the intragranular strain localization triggered during the PLC occurrence is also intense. The two other categories that are the most represented are old events located at TBs and at the interior of grains. On the other hand, the 10% of the events with the highest strain amplitude after the occurrence of the first PLC bands are old events for 88.6% of them, and 43% are near TBs. This underlines the important role played by the TB in the deformation process. Even if new intragranular events are numerous and can be intense, they only account for 9% of the events with the

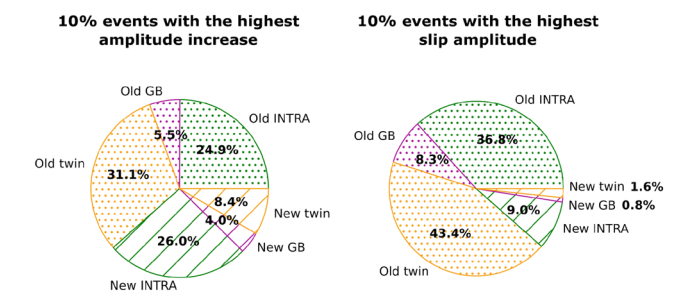


Fig. 7 Partitioning of the 10% of the events with the highest slip amplitude increase between the two loading steps of the high strain rate test (left). Partitioning of the 10% events with the highest slip amplitude after the second step of the high strain rate case (right). Old events describe the events triggered before the first interruption. New events describe the events triggered between the two loading steps. INTRA: intragranular. GB: Grain boundary. TB: Twin boundary

highest slip amplitude. Furthermore, it was found impossible to predict the location of the most intense strain localization at this stage of the deformation process. In the study case, the 10 most intense events after PLC were already present during the early stage of deformation but were between the 39th and the 365th most intense events. In other words, the most intense events before the occurrence of PLC are not necessarily the most intense after.

PLC occurrence affects the strain spatial distribution in the sample. Knowing that 70% of the events triggered during the PLC occurrence are located inside the grains, a focus has been made on their spatial distribution along the sample. Figure 8a is the full-field slip amplitude map at HSR after the occurrence of the PLC effect (3 mm long region). It is possible to notice macro-/mesoscopic strain heterogeneity due to the PLC bands captured. Figure 8b is a histogram plot of the amount of slip per area along the sample width. Each bar on the chart takes into account events contained in a 50 μm width slice of the slip amplitude map. The histogram of the first step at HSR shows a homogeneous distribution of the amount of slip

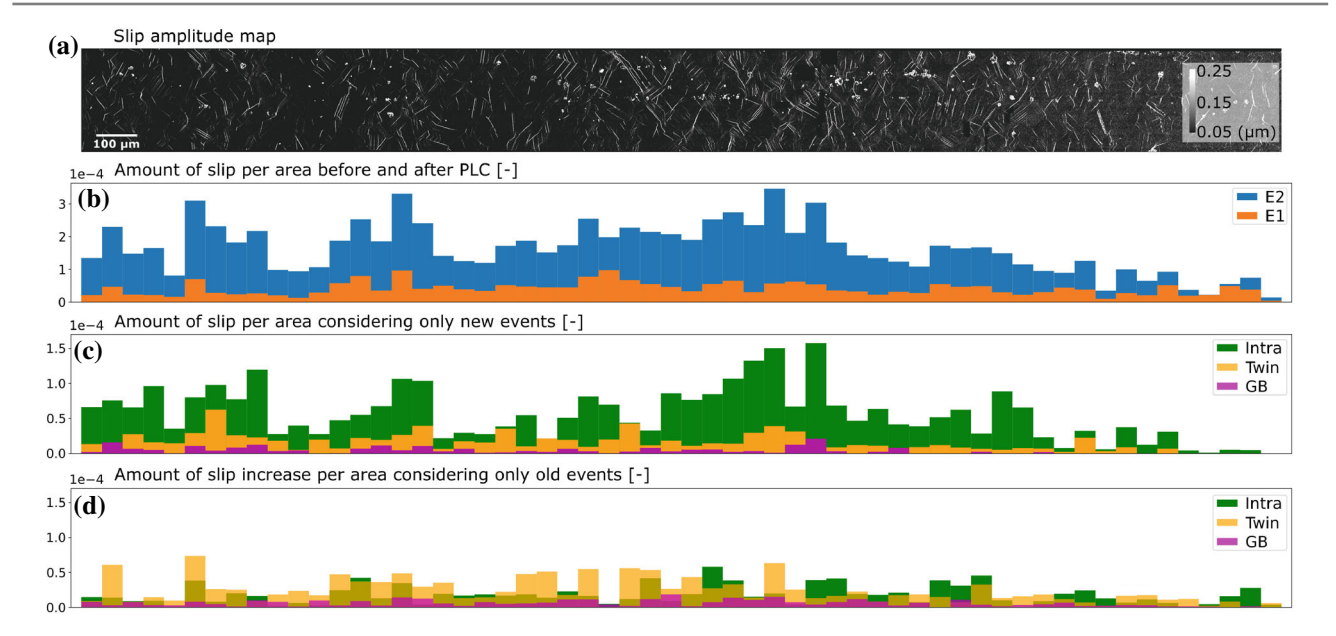


Fig. 8 Analysis of PLC at both meso- and microscale at HSR; **a** is the full-field in-plane strain localization amplitude map for the second step of HSR. **b**, **c** and **d** are histogram plots of the amount of slip/sliding per area. They are aligned with the (**a**) map. The **b** plot takes into account all the events at each step (E1 for step 1 and E2 for step 2). The **c** plot takes into account only the events triggered between the steps. The **d** plot takes into account only the events triggered before the first step. These are plotted for each microstructural feature

along the sample. In contrast, the distribution for the second step shows significant heterogeneity along the sample. The areas with a great amount of strain localization correspond to the location of PLC bands identified on both the slip amplitude (Fig. 8b) and the first third of the strain map (Fig. 4b). In the second step, data were split into two categories: old events and new events. For both categories, events were again split depending on their location, and the strain localization distribution was plotted for each location. Overlaid distributions are presented in Fig. 8c and d. In the case of the new events (Fig. 8c), the partitioning of the events is in agreement with the results presented in Fig. 5. Several strain localization events are intragranular and less are located near TBs or GBs. New events at GBs are very few but seem to be preferentially located inside the PLC bands. For those located near TBs, the strain distribution along the sample is quite homogeneous (standard deviation of 1.2×10^{-5}). In contrast, the massive amount of new intragranular events shows heterogeneity (standard deviation of 3.7×10^{-5}), and the areas of high slip amount are located inside PLC bands.

The spatial distribution plot of the old events (Fig. 8d) has the same scale as the one for the new events (Fig. 8c). This underlines, once again, that the strain added between the two steps is more localized in the form of new events than at the location of existing plastic events. In the case of old events, the spatial distribution of any location does not follow the PLC bands pattern. More strain was found at TBs and inside grains but independently of the location along the sample.

Discussion

At 650 °C, the tensile properties of Alloy 718 are known to be dependent on the strain rate. This experimental study aimed to assess this dependency at the microstructural scale. Two tensile test conditions were investigated, both at 650 °C and under vacuum: one with a strain rate of 10^{-2} s⁻¹ (HSR) and one of 10^{-4} s⁻¹ (LSR). Alloy 718 experienced Portevin-Le-Chatelier (PLC) instabilities at HSR but not at LSR. In the early stage of deformation and before the occurrence of PLC bands, differences in strain localization were evidenced between the two test conditions. At HSR and 0.07% of plastic strain, the fraction of strain located at GBs is 12%. In contrast, GBs are the location of 43% of the overall plastic strain at LSR. The strain state captured for the LSR test is slightly higher than the one of the HSR test (0.2% versus 0.07%). However, in a recent study [11], tensile tests were performed in the exact same conditions as the LSR test and showed that the fraction of strain localization at GBs slightly decreases between 0.1 and 0.5% of plastic strain. This indicates that, even if the strain state slightly differs, it is reasonable to state that a lower strain rate leads to a higher fraction of GB sliding in the overall deformation process. Thus, the PLC instabilities captured at HSR are most certainly not responsible for the small amount of GB sliding observed after their occurrence.

In the literature, the PLC phenomenon is often investigated as a macroscopic or mesoscopic phenomenon [29–31]. At HSR, PLC instabilities were also observed at both these

scales: at the macroscopic scale, with stress drops on stressstrain curves (cf. Fig. 1) and at the mesoscale, with mesoscopic inclined bands forming for the different stress drops (cf. Figs. 2, 8 and 4b). The HR-DIC calculations and the statistical analysis carried out in this work show that PLC instabilities can also be characterized at the microscale. The occurrence of PLC instabilities changed the strain partitioning. Indeed, the statistical analysis over thousands of plastic events showed that the fraction of intragranular slip bands increases with the PLC effect at the cost of a lower fraction of slip bands near TBs (cf. Fig. 5). Investigating the origins of these plastic events showed that 65% of them were triggered during the occurrence of the PLC. Most of these new events are located inside the grains and have low intensity even if some can have a particularly high slip amplitude (9% of the 10% most intense events are new events located inside the grains, as shown in Fig. 6). It was found that new intragranular slip events are preferentially triggered in the interior of the PLC bands. The high amount of intragranular slip that comes with PLC bands disturbs the macroscopic strain field. The spatial distribution of the new plastic events at GBs is a sign of this change. These new plastic events at GBs, are preferentially triggered inside the PLC bands, where the intragranular slip density is the highest. Several studies [8, 24] have established that, at intermediate and high temperatures, GB sliding can be triggered by the surrounding plastic activity, such as slip bands. This GB solicitation does not play a major role in the deformation process, as most intragranular slip bands triggered with the PLC bands have a low slip amplitude.

At the same time, TBs were also found to be the locations of high slip amplitudes. Unlike the intragranular strain localization, slip bands located near and parallel to TBs are randomly distributed along the sample. Indeed, new events located near and parallel to TBs were found inside and outside of PLC bands at HSR, and no significant difference in the amount of slip was found. Also, the amplitude increase observed at this location was found to be independent of their location along the sample. In addition, the slip events near and parallel to TBs have a great amplitude increase with the increase of macroscopic strain. One-third of the 10% events with the highest amplitude are located near TB. At 0.47% of macroscopic plastic strain, considering the 10% events with the highest slip amplitude, 43.4% are events triggered near TBs in the early stage of deformation. The amount of slip near TB at a lower strain rate is similar, as it accounts for 42.4% of the most intense events in this case. These findings are in agreement with the literature on this subject [15] and underline the important role played by the TBs in the deformation process.

In order to assess the damaging behavior, it seems necessary to take into account the numerous and intense slip events

located near TB. If the latter is independent of the strain rate, this is not the case of strain localization at GB and intragranular slip. On one hand, GBs were found to be much lesser stressed at HSR compared to LSR. Interestingly, previous work showed that in air at 650 °C, Alloy 718 shows intergranular fracture at LSR and a transgranular fracture at HSR [3]. This point might be worth further investigating. In this study, the high-strain localization at GBs at LSR could explain the higher ductility of the corresponding sample. However, in the HSR case, GBs seem to play a limited role in the deformation process as GB strain localization was found in a small fraction of the partitioning of all events, even the most intense ones. In addition, slip amplitude increase at this location was found to be lower than elsewhere. On the other hand, intragranular strain localization has an increasing share in the deformation process with the occurrence of PLC instabilities. In this study, three PLC bands were captured, and a significant number of intragranular slip events were triggered. With the increasing number of PLC bands (cf. Fig. 2), it is expected to see the fraction of intragranular strain localization increase again. At one point, the entire sample gauge will be covered with PLC bands. There, a high density of intragranular slip events homogeneously distributed along the sample can be expected. Taking into account the high slip amplitude of many of them, intragranular strain localization is expected to be a major contributor to the damage behavior of the sample.

Conclusions

HR-DIC measurements conducted at 650 °C, combined with statistical analyses, allowed for microscale characterization of PLC instabilities triggered at a high strain rate. The present work demonstrates that macroscopic PLC bands can be described as areas with a high density of intragranular slip events. At a strain rate of 10⁻⁴ s⁻¹, no PLC occurred, and a high amount of GB sliding was observed. In addition, the strain partitioning between microstructural features (GBs, TBs, and intragranularly) is homogeneously distributed across the sample. At a strain rate of 10^{-2} s⁻¹, PLC instabilities occurred, and the strain distribution along the sample is heterogenous, with PLC bands being more deformed. Inside the PLC bands, the formation of intragranular slip bands is favored. In contrast, slip near and parallel to TBs is not affected by the strain rate or PLC occurrence. At 650 °C and for both strain rates, TBs are sites of intense strain localization. The tracking of the events during the two-step test at the strain rate of 10^{-2} s⁻¹ also showed that the slip amplitude increases more at TBs than elsewhere. Finally, the damage behavior with the occurrence of PLC instabilities is expected to be driven by the large intragranular strain localization and the increasing slip amplitude at TBs.

Acknowledgements This work was supported by the European Research Council [project HT-S₄DefOx—Grant number 948007]. A [CC-BY public copyright license] has been applied by the authors to the original manuscript and will be applied to all subsequent versions up to the Author Accepted Manuscript arising from this submission, in accordance with the grant's open access conditions. The authors are grateful to the Centre National de la Recherche Scientifique (CNRS) for the mobility grant with the International Research Project denoted "CIN&MAT". RLB and JCS acknowledge the National Science Foundation (NSF award #2338346) for financial support. The authors particularly acknowledge the Raimond Castaing Microanalysis Centre (UAR 3623) for scanning electron microscopy access.

References

- H.L. Eiselstein. Metallurgy of a columbium-hardened nickelchromium-iron alloy. ASTM, 369, 1965.
- G. Greene and Charles Finfrock. Oxidation of Inconel 718 in air at high temperatures. Oxidation of Metals, 55:505–521, 2001.
- Eric Andrieu, Bertrand Max, and Bernard Viguier. Oxidation assisted intergranular cracking in Alloy 718: Effects of strain rate and temperature. AerospaceLab-iournal, 9:1–7, 2015.
- V. Garat, J.-M. Cloue, D. Poquillon, and E. Andrieu. Influence of Portevin-Le Chatelier effect on rupture mode of alloy 718 specimens. *Journal of Nuclear Materials*, 375, 2008.
- L. Fournier, D. Delafosse, and T. Magnin. Oxidation induced intergranular cracking and Portevin-Le Chatelier effect in nickel base superalloy 718. Materials Science and Engineering: A, 316, 2001.
- B.S. Rowlands, C. Rae, and E. Galindo-Nava. The Portevin-Le Chatelier effect in nickel-base superalloys: Origins, consequences and comparison to strain ageing in other alloy systems. *Progress in Materials Science*, 132, 2023.
- L. Xiao, D.L. Chen, and M.C. Chaturvedi. Shearing of γ" precipitates and formation of planar slip bands in Inconel 718 during cyclic deformation. *Scripta Materialia*, 52:603–607, 2005.
- Patrick Villechaise, Jonathan Cormier, Thomas Billot, and José Mendez. Mechanical behavior and damage processes of Udimet 720Li: Influence of localized plasticity at grain boundaries. *TMS*, pages 15–24, 2012.
- 9. A. Soula, D. Locq, D. Boivin, and et al. Quantitative evaluation of high temperature deformation mechanisms: a specific microgrid extensometry technique coupled with EBSD analysis. *J Mater Sci*, 45:5649–5659, 2010.
- J.L. Walley, R. Wheeler, M.D. Uchic, and al. In-situ mechanical testing for characterizing strain localization during deformation at elevated temperatures. *Exp Mech*, 52:405–416, 2012.
- D. Texier, J. Milanese, M. Jullien, J. Genée, J.C. Passieux, D. Bardel, E. Andrieu, M. Legros, and J.C. Stinville. Strain localization in alloy 718 ni-based superalloy: from room temperature to 650 °C. Acta Materialia, 2024.
- F. Bourdin, J.C. Stinville, M.P. Echlin, P.G. Callahan, W.C. Lenthe, C.J. Torbet, D. Texier, F. Bridier, J. Cormier, P. Villechaise, T.M. Pollock, and V. Valle. Measurements of plastic localization by heaviside-digital image correlation. *Acta Materialia*, 157:307–325, 2018
- S. Hémery, J-C. Stinville, F. Wang, M-A. Charpagne, M.G. Emigh, T.M. Pollock, and V. Valle. Strain localization and fatigue crack formation at (0001) twist boundaries in titanium alloys. *Acta Materialia*, 219, 2021.

- F. Di Gioacchino and J. Quinta da Fonseca. Plastic strain mapping with sub-micron resolution using digital image correlation. *Exp Mech*, 53:743–754, 2013.
- J.C. Stinville, N. Vanderesse, F. Bridier, P. Bocher, and TM. Pollock. High resolution mapping of strain localization near twin boundaries in a nickel-based superalloy. *Acta Materialia*, 98:29–42, 2015.
- R. Jiang, F. Pierron, S. Octaviani, and P.A.S. Reed. Characterisation of strain localisation processes during fatigue crack initiation and early crack propagation by SEM-DIC in an advanced disc alloy. *Materials Science and Engineering: A*, 699, 2017.
- J.C. Stinville, P.G. Callahan, M.A. Charpagne, M.P. Echlin, V. Valle, and T.M. Pollock. Direct measurements of slip irreversibility in a nickel-based superalloy using high resolution digital image correlation. *Acta Materialia*, 186, 2020.
- M.A. Charpagne, J. Hestroffer, A.T. Polonsky, M.P. Echlin, Damien Texier, and al. Slip localization in Inconel 718: a three-dimensional and statistical perspective. *Acta Materialia*, 215, 2021.
- J.C. Stinville, W.C. Lenthe, M.P. Echlin, P.G. Callahan, D. Texier, and T.M. Pollock. Microstructural statistics for fatigue crack initiation in polycrystalline nickel- base superalloys. *International Journal of Fracture*, 208:221–240, 2017.
- F. Bridier, J.-C. Stinville, N. Vanderesse, P. Villechaise, and P. Bocher. Microscopic strain and crystal rotation measurement within metallurgical grains. *Key Engineering Materials*, 208:493– 496, 2013.
- Z. Zhang, Z. Yang, S. Lu, and al. Strain localisation and failure at twin-boundary complexions in nickel-based superalloys. *Nat Commun*, 11, 2020.
- Z. Chen and S.H. Daly. Active slip system identification in polycrystalline metals by digital image correlation (DIC). *Exp Mech*, 57:115-127, 2017.
- A.P. Sutton and R.W. Balluffi. Interfaces in crystalline materials. Monographs on the Physics and Chemistry of Materials., 1996.
- 24. M.A. Linne, A. Venkataraman, M.D. Sangid, and al. Grain boundary sliding and slip transmission in high purity aluminum. *Exp Mech*, 59:643–658, 2019.
- J.H. Liu, N. Vanderesse, J.-C. Stinville, T.M. Pollock, P. Bocher, and al. In-plane and out-of-plane deformation at the sub-grain scale in polycrystalline materials assessed by confocal microscopy. *Acta Materialia*, 169:260–274, 2019.
- A. Rouwane, D. Texier, S. Hemery, J.C. Stinville, and Q. Sirvin. Strain localization in Ti and Ti-alloys using three-dimensional topographic imaging. World Titanium Conference, 2023.
- F Bachmann, Ralf Hielscher, and Helmut. Schaeben. Texture Analysis with MTEX-Free and Open Source Software Toolbox. Solid State Phenomena, 160, 2010.
- M.A. Charpagne, J.C. Stinville, Andrew Polonsky, M. Echlin, and T. Pollock. A Multi-modal data merging framework for correlative investigation of strain localization in three dimensions. *JOM*, 2021.
- P. Penning. Mathematics of the Portevin-le Chatelier Effect. Acta Metallurgica, 20:1169–1175, 1972.
- A. Le Chatelier. Influence du temps et de la température sur les essais au choc. Rev. Met. Paris, 6:914–917, 1909.
- Yanke Liu, Yulong Cai, Chenggang Tian, Guoliang Zhang, Guoming Han, Shihua Fu, Chuanyong Cui, and Qingchuan Zhang. Experimental investigation of a portevin-le chatelier band in ni-co-based superalloys in relation to γ' precipitates at 500°c. *Journal of Materials Science & Technology*, 49:35–41, 2020.